15

Preliminary calculation of sensitivity of detectors for the future space experiment „Sun-Terahertz“

© M.V. Philippov, V.S. Makhmutov, V.I. Logachev, M.V. Razumeyko

Lebedev Physical Institute, Russian Academy of Sciences,
119991 Moscow, Russia
e-mail: office@lebedev.r, mfilippov@frtk.ru

Received July 5, 2023
Revised July 12, 2023
Accepted July 12, 2023

The paper briefly describes the goals and objectives of the planned space experiment „Sun−Terahertz“ aboard the Russian Segment of the ISS. The experiment is aimed at studying solar radiation in the unexplored terahertz range at frequencies of 1012 . . . 1013 Hz, obtaining new data on terahertz radiation from the sun, solar active regions and solar flares. The main components of the optical path of scientific equipment are considered. With the help of the Blackbody Simulator and the Single-Channel Model, the detectors of scientific equipment were calibrated, the influence of the quality of the optical surface of the telescope mirrors on the detector signal amplitude in the terahertz range was studied, and a preliminary assessment of the detector sensitivity was carried out.

Keywords: Sun, solar flares, terahertz radiation, optical system.

DOI: 10.61011/TP.2023.09.57369.167-23

Introduction

The space experiment „Sun-Terahertz“ on board the Russian segment of the ISS is aimed at studying the Sun's radiation in the unexplored terahertz range at frequencies of $10^{12}-10^{13}$ Hz [1]. The main goal of the experiment — to obtain new data on terahertz radiation from the Sun, solar active regions, and solar flares [2–6]. These data are necessary to elucidate the nature of solar activity, to determine the physical mechanism of acceleration of charged particles on the Sun and other astrophysical objects.

In the present paper, the main components of the optical path of scientific instruments (hereinafter — SI) are considered. With the help of a black body simulator and a single-channel model, the detectors of the scientific equipment were calibrated, the influence of the quality of the optical surface of the telescope mirrors on the sensitivity range of the detectors in the terahertz range was investigated, and a preliminary evaluation of the sensitivity of the detectors was carried out.

The launch of the Sun-Terahertz space experiment is scheduled for 2024−2025.

1. Basic equipment

The developed equipment (Fig. 1) is a set of eight detectors sensitive to radiation of different frequencies — 0.4, 0.8, 1.0, 3.0, 5.0, 7.0, 10.0 and 12.0 THz. Each detector includes:

— an optical telescope [7] that concentrates radiation at an optoacoustic transducer (OAT) through a system of filters and an optical chopper;

— a system of sequential filters that passes radiation over a given frequency range for each detection module, thus providing selectivity;

— an optical interrupter that modulates the radiation at the receiver's input window at a frequency of 10 or 20 Hz;

— OAT that is part of the radiation receiver.

2. Auxiliary equipment

A single-channel layout — a device for testing scientific instrumentation detectors, within which the telescope, filters, and receiver under test are mounted.

Blackbody imitator (BBI) is designed to verify the performance of the Sun-Terahertz scientific HA during ground-

Figure 1. Appearance of HA„Sun-Terahertz“ (three-dimensional model) from the front panel side

Table 1. Comparison of set and measured temperatures of the BBI transmitter

BBI transmitter temperature by According to the meter-regulator t_{bb} (K)	BBI transmitter temperature according to the infrared data of pyrometer t_p (K)	$\frac{t_{bb}-t_p}{t_{bb}} \cdot 100\%$
373	363	2.68
473	455	3.80
573	546	4.71
673	636	5.49
773	721	6.72
873	805	7.79

based experimental testing, namely, to carry out checks, adjustments and calibrations of the detection modules. The BBI consists of two units: the BBI transmitter and the control and power supply unit.

The principle of operation of the BBI is to generate an energy flow in the terahertz wavelength range using a heated ceramic radiator and an off-axis parabolic mirror.

A Kelvin-Compact D [8] infrared pyrometer is used as a means of controlling the temperature of the BBI emitter, which is used to compare the temperature of the BBI emitter according to the controller and the temperature measured by the pyrometer from the BBI surface. Table 1 shows the results of measurements. The difference between the set and measured temperature values of the BBI emitter in the section 373 to 873 K does not exceed 8% and is probably due to the characteristics of the emitting element (an AlN-230 alumino-nitride ceramic puck with thermal conductivity 230 W/(m·K) and a degree of blackness in the terahertz wavelength range not less than 0.88).

3. Radiation receivers

„The Golay" cell OAT-1P [9] belongs to the class of non-selective uncooled receivers. The spectral sensitivity of the OAT mainly depends on the characteristics of the input window. In OAT GC-1P, the inlet window is made of high-density polyethylene (HDPE).

The receiver (together with the optical interrupter) is a source of a variable quasi-sinusoidal bipolar signal, the points of extrema of which correspond to the closing-opening positions of the optical interrupter blades.

In further analysis, the signal spread — the difference between two nearby signal extrema–is used:

$$U_i = V_{2i-1} - V_{2i}, \tag{1}$$

where U_i — signal magnitude i, [mV]; V_{2i-1} — local extremum $2i-1$, [mV]; V_{2i} — local extremum $2i$, [mV]; i — measurement number.

For definiteness, point V_{2i-1} corresponds to open optical breaker blades and point V_{2i} — closed blades.

Table 2. Characteristics of tested filter systems

№	Filter	$\nu_{\max}$, THz	$t_{0.7}$	$\Delta\nu_{0.7}$, THz
1	HDPE+LPF+BPF 0.4	0.37	0.38	0.38
2	HDPE+LPF+BPF 0.8	0.79	0.44	0.07
3	HDPE+LPF+BPF 1.0	1.00	0.38	0.10
4	HDPE+LPF+BPF 3.0	2.97	0.22	0.40
5	HDPE+LPF+BPF 5.0	4.82	0.16	0.62
6	HDPE+LPF+BPF 7.0	6.78	0.06	1.26
7	HDPE+LPF+BPF 10.0	9.93	0.05	0.81
8	HDPE+LPF+BPF 12.0	11.17	0.03	0.52

4. Filter system

The optical path of the Sun-Terahertz detectors includes a filter system consisting of the following components:

— cutoff filter (LPF) [10] designed to let terahertz radiation through and block short wavelengths;

— bandpass filter (BPF) [11] to form the desired detector bandwidth in the terahertz range.

Characteristics of filter systems (tested set for 8 channels) are given in Table 2. The -first column contains the channel numbers, the second column — the name of the filters used, the third column — the measured frequency of maximum passband (center frequency), the fourth column — the passband coefficient at 0.7 of maximum, and the fifth column — the filter bandwidth.

5. Sensitivity of detectors

Radiation flux from the BBI transmitter passing through the input window of the receiver (without taking into account the influence of the optical quality of the telescope

mirror surface) Φ_r, is equal to

$$\Phi_r(T) = S_{tel} \int_{\nu_1}^{\nu_2} d(\nu) r(\nu, T) t_{res}(\nu) d\nu, \qquad (2)$$

where ν — radiation frequency, [Hz]; T — temperature of a completely black body, [K]; $t_{res}(\nu)$ — the resulting transmission coefficient of the filter system and the OAT input window; $r(\nu, T)$ — spectral density of radiation per unit area in the frequency range(ν; $d\nu$), W/(m^2·Hz); $d(\nu)$ — the ratio of the radiation flux falling on the input window of the receiver to the radiation flux falling on the input window of the telescope, resulting from diffraction losses on the mirrors [7]; $S_{tel} = 3.84 \cdot 10^{-3}$ m^2 — the area of the input window of the telescope [7].

The dependence of the receiver output signal on the temperature of the BBI transmitter was obtained using the bench (Fig. 2), which was assembled on the basis of a single-channel model. A receiver, an optical interrupter at 20 Hz, a telescope (with smooth mirrors), a set of filters (a cutoff filter LPF23.1 and one bandpass filter BPF at 0.4, 0.8, 1.0, 3.0, 5.0, 7.0, 10.0 or 12.0 THz) were installed inside the single-channel layout. The receiver signal is input to the USB oscilloscope input. The computer generates a data file in CSV format with a time sampling of 1 ms for an interval of at least 10 min. With the help of the program-processor the local extrema and signal spread for each period of oscillation of the optical interruption are calculated, as well as the maximum, minimum and arithmetic mean values of the signal spread for the measurement interval and its standard deviation.

The average values of the receiver signal sweep are further used to calculate the correlation between the signal sweep and the BBI transmitter temperature using the least-square method (LSM).

Fig. 3 shows the dependence of the receiver signal sweep (U, [mV]) on the temperature of the transmitter BBI (T, [K]) with the BPF 0.4 bandpass filter set. Signal sweep data are obtained by averaging the measured values over

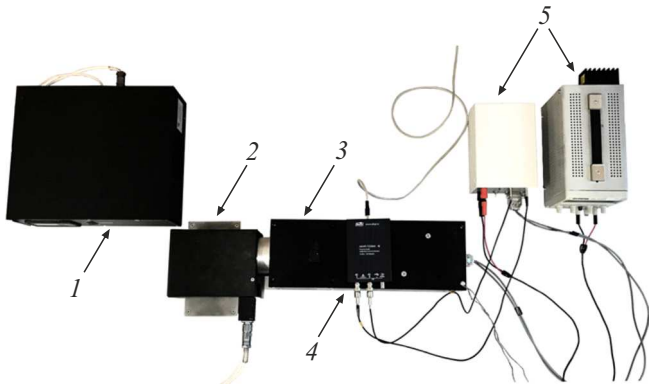

Figure 2. Assembling the single-channel layout and black body simulator: *1* — BBI control and power supply; it 2 — BBI emitter; *3* — single-channel mock-up; *4* — ADC; *5* — power supplies

.

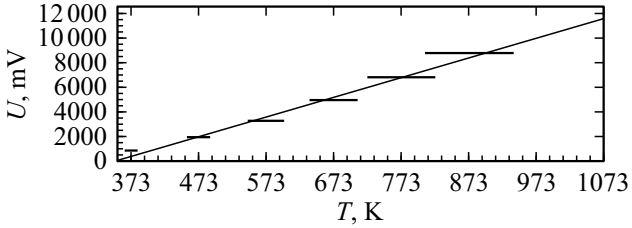

Figure 3. Dependence of the receiver signal sweep (U, [mV]) on the BBI transmitter temperature (T, [K]) with the BPF 0.4. bandpass filter set.

a time period of at least 10 min. The black horizontal segments — the magnitude of the systematic error in the target value of the IFT transmitter surface temperature. The standard deviation of the signal spread does not exceed the thickness of horizontal lines. The grey straight line — approximation of the data by the LSM.

Table 3 summarizes the results for each channel. The first column contains the channel numbers, the second column — the angular coefficients ($a_0(\nu)$, [mV/K]) of the approximating straight lines, the third column — the free terms ($b_0(\nu)$, [mV]), and the fourth column — the coefficient of determination (R_0^2).

Thus, the dependence of the receiver signal sweep on the temperature of the IFT transmitter can be represented as follows

$$U(T) = aT + b, \qquad (3)$$

where a — angular coefficient of the approximating straight line, [mV/K]; b — free term of the approximating straight line, [mV].

In order to provide additional scattering of radiation in the visible range of the spectrum, the mirrors undergo a special surface treatment with lapping withAl_2O_3 powder of 600 to 1200 grain size and short-term etching in NaOH solution followed by washing in deionized water.

A similar technique was also used in the SOLAR-T [12] experiment.

Columns five through seven of Table 3 show the data obtained from measurements with rough mirrors.

In approximation that the reflectance for an untreated (smooth) mirror $\rho = 1$, we can write

$$\rho_t(\nu, T) = \frac{U_1(\nu, T)}{U_0(\nu, T)} \approx \frac{a_1(\nu)}{a_0(\nu)}, \qquad (4)$$

where $\rho_t(\nu, T)$ — the spectral reflectance of the mirror system in the telescope; $U_0(\nu, T)$ — the receiver signal magnitude with smooth mirrors installed in the telescope, [mV]; $U_1(\nu, T)$ — the receiver signal magnitude with rough mirrors installed in the telescope, [mV]. Since the telescope has two mirrors [7], the spectral reflectance of a single mirror surface is

$$\rho_m(\nu) = \sqrt{\rho_t(\nu)}. \qquad (5)$$

Table 3. Size distribution of stainless steel granules

№	$a_0(\nu)$, mV/K	$b_0(\nu)$, mV	R_0^2	$a_1(\nu)$, mV/K	$b_1(\nu)$, mV	R_1^2	$\rho_t(\nu)$	$\rho_m(\nu)$
1	16.0 ± 0.8	-5500.3 ± 538.0	0.99	11.7 ± 0.2	-3772.0 ± 113.1	0.99	0.73	0.85
2	12.9 ± 0.8	-4614.8 ± 485.7	0.99	8.7 ± 0.1	-2877.2 ± 90.8	0.99	0.67	0.82
3	13.1 ± 0.6	-4608.2 ± 360.9	0.99	8.3 ± 0.3	-2794.3 ± 211.6	0.99	0.63	0.79
4	18.9 ± 1.1	-6941.4 ± 703.0	0.99	11.3 ± 0.2	-3782.7 ± 138.7	0.99	0.60	0.77
5	33.1 ± 2.7	-12435.4 ± 1741.6	0.97	18.4 ± 0.6	-6132.8 ± 389.8	0.99	0.56	0.75
6	35.9 ± 2.3	-13154.8 ± 1492.6	0.98	18.4 ± 0.6	-6186.2 ± 358.4	0.99	0.51	0.71
7	26.0 ± 1.7	-9272.0 ± 1092.0	0.98	14.1 ± 0.2	-4600.5 ± 103.1	0.99	0.54	0.74
8	39.1 ± 2.2	-14015.5 ± 1423.9	0.99	21.2 ± 0.5	-7107.8 ± 349.9	0.99	0.54	0.74

The eighth column of Table 3 shows the spectral reflectance of the telescope $\rho_t(\nu)$, and the ninth column — the spectral reflectance of one mirror $\rho_m(\nu)$.

Taking into account the influence of the quality of the optical surface of the telescope mirrors, the radiation flux passing through the input window of the receiver Φ_r is as follows

$$\Phi_r(T) = S_{tel} \int_{\nu_1}^{\nu_2} \rho_t(\nu) d(\nu) r(\nu, T) t_{res}(\nu) d\nu, \qquad (6)$$

where $\rho_t(\nu)$ — the spectral reflectance of the mirror system in the telescope. Taking into account the relation (3), the Planck [13] formula can be represented in the following form

$$r(\nu, U) = \frac{2\pi h \nu^3}{c^2} \frac{1}{e^{\frac{ah\nu}{k(U-b)}} - 1}, \qquad (7)$$

where $r(\nu, U)$ — spectral density of radiation per unit area in the frequency interval $(\nu;\ d\nu)$, [W/(m^2·Hz)]; ν — frequency of radiation, [Hz].

$\Phi_d(T)(J)$ radiation flux arriving at the entrance window of the telescope

$$\Phi_d(T) = S_{tel} \int_{\nu_1'}^{\nu_2'} r(\nu, T) d\nu. \qquad (8)$$

The efficiency of the detector optical path (telescope, filter system, receiver input window) can be estimated as the ratio of the radiation flux at the receiver to the radiation flux at the telescope in the bandwidth of the detector filter system — Φ_r/Φ_d . To do this, expressions (6) and (8) must be integrated at frequencies within the passband of the filter system for each detector (Table 2.):

$$\nu_1 = \nu_{\max} - \Delta\nu_{0.7}/2;$$
$$\nu_2 = \nu_{\max} + \Delta\nu_{0.7}/2. \qquad (9)$$

The dynamic range of the output sweep of the receiver ΔU, is primarily determined by the amplifier design and is approximately 27 V. By substituting $U_0 = 0$ V and $U_1 = 27$ V into (6)–(8) with condition (9), the values of the radiation fluxes at the receiver $\Phi_r(U_0)$ and $\Phi_r(U_1)$, and the values of the radiation fluxes at the input window of the detector telescope $\Phi_d(U_0)$ and $\Phi_d(U_1)$ are obtained.

The sensitivity of the detectors is estimated as the ratio $\Delta U/\Delta\Phi_d$, where $\Delta U = U_1 - U_0$, [V]; $\Delta\Phi_d = \Phi_d(U_1) - \Phi_d(U_0)$, [W].

From the relationship (3), the absolute error of the signal sweep due to the design of the IFT transmitter is expressed:

$$\sigma_{BBI} \approx \sigma_a T + \sigma_T a + \sigma_b, \qquad (10)$$

where σ_{BBI} — absolute error in the signal sweep $U(T)$ of the receiver due to the deviation of the actual BBI transmitter temperature from the set value, [mV]; σ_a — absolute error a, [mV/K]; σ_b — absolute error b, [mV]; σ_T — absolute temperature error T of the BBI transmitter, [K].

Consider the case where the total absolute error σ_U of the receiver signal sweep depends only on the accuracy of the BBI transmitter temperature setting:

$$\sigma_U \approx \sigma_{BBI}.$$

Absolute error of spectral density of radiation per unit area $r(\nu, U)$:

$$\sigma_R = \frac{\partial(r(\nu, U))}{\partial U} \sigma_U,$$

$$\sigma_R = \frac{2\pi h \nu^3}{c^2} \frac{\frac{ah\nu}{k} \cdot e^{\frac{ah\nu}{k(U-b)}}}{\left(e^{\frac{ah\nu}{k(U-b)}} - 1\right)^2 (u-b)^2} \sigma_U. \qquad (11)$$

By substituting (11) into (6) and (8), expressions for absolute errors of radiation fluxes at the receiver and at the input window of the detector telescope, respectively, are obtained

$$\sigma_r = S_{tel} \int_{\nu_1}^{\nu_2} \rho_t(\nu) d(\nu) \sigma_R(\nu, U) t_{res}(\nu) d\nu, \qquad (12)$$

$$\sigma_d = S_{tel} \int_{\nu_1}^{\nu_2} \sigma_R(\nu, U) d\nu. \qquad (13)$$

Table 4. Results of calculating the sensitivity of the detectors

№	$\Phi_r(0\,\mathrm{V})$, W	$\Phi_r(27\,\mathrm{V})$, W	$\Phi_d(0\,\mathrm{V})$, W	$\Phi_d(27\,\mathrm{V})$, W	Φ_r/Φ_d	$\Delta U/\Delta\Phi_d$, V/W
1	$(1.4 \pm 0.3) \cdot 10^{-6}$	$(8.4 \pm 1.2) \cdot 10^{-6}$	$(5.1 \pm 0.9) \cdot 10^{-6}$	$(3.1 \pm 0.5) \cdot 10^{-5}$	$(2.7 \pm 1.0) \cdot 10^{-1}$	$(1.1 \pm 0.5) \cdot 10^{6}$
2	$(1.7 \pm 0.4) \cdot 10^{-5}$	$(1.3 \pm 0.2) \cdot 10^{-4}$	$(5.5 \pm 1.1) \cdot 10^{-5}$	$(3.9 \pm 0.6) \cdot 10^{-4}$	$(3.2 \pm 1.3) \cdot 10^{-1}$	$(8.0 \pm 3.4) \cdot 10^{4}$
3	$(3.4 \pm 0.5) \cdot 10^{-5}$	$(2.4 \pm 0.3) \cdot 10^{-4}$	$(1.3 \pm 0.2) \cdot 10^{-4}$	$(8.8 \pm 1.2) \cdot 10^{-4}$	$(2.7 \pm 0.8) \cdot 10^{-1}$	$(3.6 \pm 1.3) \cdot 10^{4}$
4	$(6.2 \pm 1.4) \cdot 10^{-4}$	$(3.6 \pm 0.6) \cdot 10^{-3}$	$(3.9 \pm 0.9) \cdot 10^{-3}$	$(2.3 \pm 0.4) \cdot 10^{-2}$	$(1.6 \pm 0.7) \cdot 10^{-1}$	$(1.5 \pm 0.7) \cdot 10^{3}$
5	$(1.6 \pm 0.6) \cdot 10^{-3}$	$(6.2 \pm 1.4) \cdot 10^{-3}$	$(1.5 \pm 0.5) \cdot 10^{-2}$	$(5.8 \pm 1.3) \cdot 10^{-2}$	$(1.1 \pm 0.8) \cdot 10^{-1}$	$(6.2 \pm 5.3) \cdot 10^{2}$
6	$(2.0 \pm 0.6) \cdot 10^{-3}$	$(8.4 \pm 1.8) \cdot 10^{-3}$	$(4.9 \pm 1.5) \cdot 10^{-2}$	$(2.1 \pm 0.4) \cdot 10^{-1}$	$(4.0 \pm 2.5) \cdot 10^{-2}$	$(1.7 \pm 1.3) \cdot 10^{2}$
7	$(1.3 \pm 0.5) \cdot 10^{-3}$	$(8.8 \pm 1.8) \cdot 10^{-3}$	$(5.0 \pm 2.0) \cdot 10^{-2}$	$(3.5 \pm 0.7) \cdot 10^{-1}$	$(2.5 \pm 2.0) \cdot 10^{-2}$	$(9.1 \pm 5.6) \cdot 10^{1}$
8	$(7.7 \pm 2.8) \cdot 10^{-4}$	$(4.0 \pm 1.0) \cdot 10^{-3}$	$(3.7 \pm 1.4) \cdot 10^{-2}$	$(2.0 \pm 0.4) \cdot 10^{-1}$	$(2.0 \pm 1.5) \cdot 10^{-2}$	$(1.7 \pm 1.2) \cdot 10^{2}$

Table 4 summarizes the results of detector sensitivity calculations. The first column shows the channel numbers, the second column — the radiation fluxes at the receiver at the $U_0 = 0\,\mathrm{V}$ output sweep, the third column — the radiation fluxes at the receiver at the $U_1 = 27\,\mathrm{V}$ output sweep, in the fourth column — the radiation fluxes at the telescope input window at the receiver output signal sweep $U_0 = 0\,\mathrm{V}$, in the fifth column — the radiation fluxes at the telescope input window at the receiver output signal sweep $U_1 = 27\,\mathrm{V}$, in the sixth column — the detector optical path efficiency, in the seventh column — the detectors sensitivity.

Conclusion

The spectral reflectance of the HA telescope mirrors in the frequency range of interest from 0.4 to 12 THz was determined experimentally, which further allowed us to calculate the efficiency of the optical path of the detectors and their sensitivity.

The telescope efficiency decreases with increasing frequency from about 30 (detector at 0.4 THz) to 2% (detector at 12.0 THz), which is a consequence of the decreasing filter system bandwidth, but the bandwidth increases, which generally compensates for the decreasing filter system efficiency. As the bandwidth of the channel increases, its resolution decreases.

The sensitivity of the detectors drops by 4 orders of magnitude, which is mainly compensated by the large radiation fluxes at these frequencies.

It should also be noted that in order to increase the calibration accuracy, i.e., to refine the dependence $U(T)$, it is necessary to further calibrate the receivers both at different BBI temperatures and at variations in the intrinsic temperature of the receivers to determine the temperature dependence of the OAT „Golay cell“.

Conflict of interest

The authors declare that they have no conflict of interest.

References

[1] E.V. Kalinin, M.V. Philippov, V.S. Makhmutov, V.S. Maksumov, Yu.I. Stozhkov, A.A. Kvashnin, G.N. Izmailov, V.V. Ozolin. Cosmic Research, **59** (1), 1 (2021). DOI: 10.1134/S0010952521010032

[2] P. Kaufmann, J.-P. Raullin, C.G.G. de Castro, H. Levato, D.E. Gary, J.E.R. Costa, A. Marun, P. Pereyra, A.V.R. Silva, E. Correia. Astrophys. J., **603**, L121 (2004). DOI: 10.1086/383186

[3] P. Kaufmann. AIP conference Proceedings, **374**, 379 (1996). DOI: 10.1063/1.50945

[4] P. Kaufmann, C.G.G. Castro, V.S. Makhmutov, J.-P. Raulin, R. Schwenn, H. Levato, M. Rovira. Journal of Geophysical Research, **108**(A7), 1280 (2003). DOI: 10.1029/2002JA009729

[5] S. Krucker, C.G.G. Castro, H.S. Hudson, G. Trottet, T. Bastian, A. Hales, J.K. Sparova, K.-L. Klein, M. Kretzschmar, T. Luthi, A.L. Mackinnon. S. Pohjolainen, S.M. White. Astron. Astrophys. Rev., **21**, 58 (2013). DOI: 10.1007/s00159-013-0058-3

[6] T. Luthi, A. Magun, M. Miller. Astron. Astrophys., **415**, 1123 (2004). DOI: 10.1051/0004-6361:20034624

[7] A.A. Kvashnin, V.I. Logachev, M.V. Philippov, V.S. Makhmutov, O.S. Maksumov, Y.I. Stozhkov, E.V. Kalinin, A.A. Orlov, V.V. Ozolin, G.N. Izmaylov, A.G. Gaifutdinova, O.Y. Krivolapova. Kosmicheskaya tekhnika i tekhnologii, **4** (35), 22 (2021) (in Russian). DOI: 10.33950/spacetech-2308-7625-2021-4-22-30

[8] *Characteristics of infrared pyrometer Kelvin-Compact D.* Electronic resource. URL: https://zaoeuromix.ru/files/docs/KelvinD.pdf (date of access 15.01.23)

[9] *Characteristics of OAT „Golay cell“* Electronic resource. Available at: http://www.tydexoptics.com/ru/ (date of access 15.01.23)

[10] *Characteristics of LPF23.1* cut-off filters Electronic resource. Available at: http://www.tydexoptics.com/pdf/ru/THz_Low_Pass_Filter.pdf (date of access 15.01.23)

[11] *Characteristics of BPF* cut-off filters Electronic resource. Available at: http://www.tydexoptics.com/ru/products/tgc-ustrojstva/thz_band_pass_filter/ (date of access 15.01.23)
[12] P. Kaufmann, R. Marcon, A. Abrantes, E.C. Bortolucci, L.O.T. Fernandes, G.I. Kropotov, A.S. Kudaka, N. Machado, A. Marun, V. Nikolaev, A. Silva, C.S. da Silva, A. Timofeevsky. Exp Astron, **37**, 579 (2014). DOI: 10.1007/s10686-014-9389-y
[13] D.V. Sivukhin, *Obshchiy kurs fiziki, t. 3. Optics* (Fizmatlit MIPT, M., 2002)

Translated by Y.Deineka